Combustion and Flame 271 (2025) 113800

Contents lists available at ScienceDirect

Combustion and Flame

journal homepage: www.sciencedirect.com/journal/combustion-and-flame

Three-dimensional dynamics of unstable lean premixed hydrogen-air flames: Intrinsic instabilities and morphological characteristics

Yu Xie, Junfeng Yang *, Pervez Ahmed, Benjamin John Alexander Thorne, Xiaojun Gu

School of Mechanical Engineering, University of Leeds, Leeds LS2 9JT, UK

ARTICLE INFO

Keywords:
Self-acceleration
Swinging laser sheet technique
Flame surface area
3D flame visualization

ABSTRACT

The 3D swinging laser sheet technique was employed to study the development and morphological characteristics of premixed hydrogen-air unstable flames in a spherical explosion vessel. Pressure dependencies for laminar flame propagation were sought to exploit the role of the Darrieus-Landau (DL) and Thermal-diffusive (TD) instabilities in the unstable self-accelerating flame regime. A sufficiently low Markstein number, as a consequence of the increased pressure, leads to more cracking and smaller cells over the flame surface. The degree of wrinkling on the flame surface is proportional to the increase in flame burning velocity, a relationship that holds true for low pressures but is not applicable under high pressures. External turbulence can significantly alter the extent of flame surface wrinkling even at low root mean square velocities, producing a more wrinkled flame surface compared to intrinsic cellularity, and distinctly affecting flame dynamics. The increased wrinkling and flame speed due to external turbulence can be attributed to the synergistic effects between thermo-diffusive instabilities and turbulence, resulting in higher fuel consumption rates per flame surface area and the formation of finger-like structures that enhance flame displacement speed in curved segments. The parameters, ϵ, deviation of the Lewis number from a critical value, and ω_2, obtained through classical linear stability analysis, display a clear linear relationship with the ratio of the wrinkled surface area observed in planar flames. This study enhances the understanding of hydrogen flame instabilities, which is crucial for preventing explosions in hydrogen storage and utilization, and provides valuable insights into flame dynamics, supporting the design of safer and more efficient hydrogen-fueled engines and turbines.

1. Introduction

Using hydrogen, a carbon-free, clean, and renewable fuel, is a practical way to reduce greenhouse gas emissions, and achieve carbon neutrality. The global objectives for achieving net-zero emissions by 2050 have sparked significant interest in hydrogen as a combustion fuel [1]. Firstly, hydrogen is known for its unique thermophysical properties, including high molecular diffusivity and fast burning velocity [2]. Burning hydrogen in a lean premixed mode can help control flame speeds, reduce exhaust gas temperatures, and lower NOx emissions. However, lean premixed hydrogen flames are subject to thermo-diffusive instabilities [3,4], causing the initially smooth laminar flame front to wrinkle. This results in an increased overall flame surface area and global flame propagation speed [5,6]. This phenomenon may potentially progress to supersonic behaviour through a process known as deflagration-to-detonation transition (DDT) [7,8]. Understanding the origins and scope of hydrogen flame instabilities is essential for mitigating these explosion risks. Mechanisms underlying fast flame propagation and the more complex flame-flow interactions due to intrinsic instability require further investigation. A commonly utilized correlation for self-accelerating flames is as follows:

$$S_n = \frac{dr}{dt} = A \cdot \alpha \cdot t^{\alpha-1} \tag{1}$$

where $r = A \cdot t^{\alpha}$, r is the flame radius, t is the time elapsed after spark ignition, A is an empirical constant, α denotes acceleration exponent, d, fractal excess, is expressed as: $d = (\alpha - 1)/\alpha$ when assuming the increase in flame speed is proportional to the increase in the flame front area. Accurate measurements of the acceleration exponent α and fractal excess d of the flame are imperative for comprehending the self-acceleration mechanism [9,10]. In addition, the phenomenon of combustion acceleration due to flame-generated disturbances or turbulence arising from the development of flame instabilities has been extensively studied [11,12]. To comprehend the connection between

* Corresponding author.
E-mail address: J.Yang@leeds.ac.uk (J. Yang).

https://doi.org/10.1016/j.combustflame.2024.113800
Received 27 April 2024; Received in revised form 10 October 2024; Accepted 11 October 2024
Available online 23 October 2024

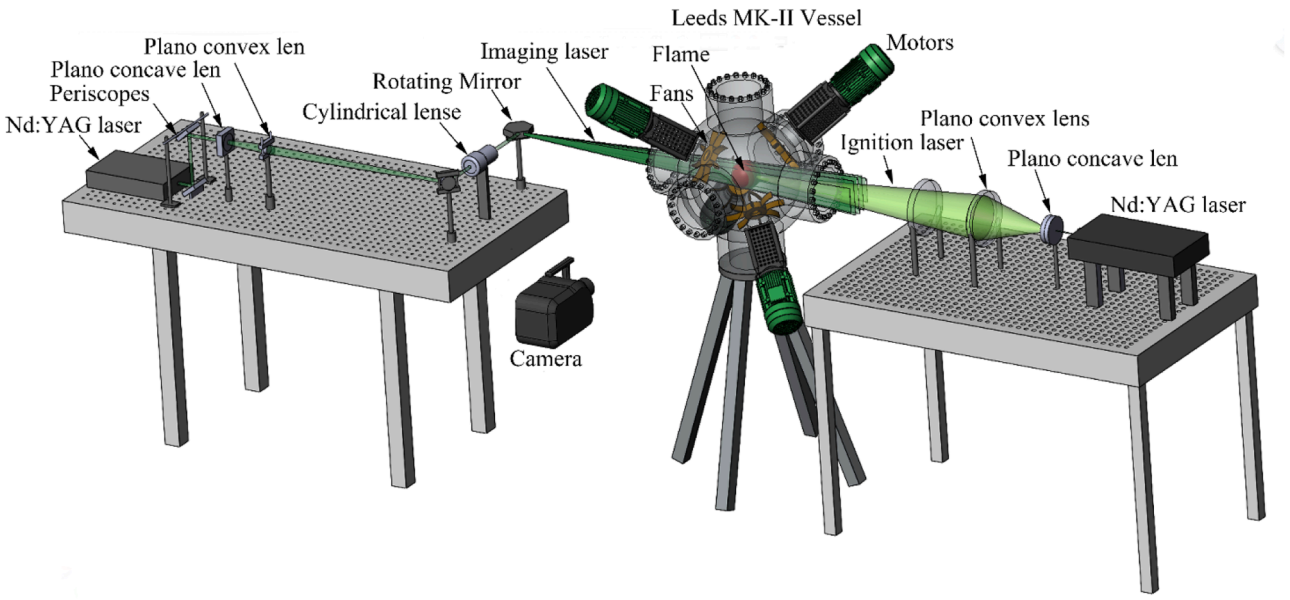

Fig. 1. Schematic of the MK-II fan-stirred combustion vessel equipped with a 3D swinging laser sheet system.

flame-generated disturbance (or turbulence) and external turbulence, some researchers employ either LDV (Laser Doppler Velocimetry) [13] or PIV (Particle Image Velocimetry) techniques [14,15].

The expansion of the flame cell, followed by its division into smaller cells due to equilibrium instability, leads to a self-similar fractal characteristic of the flame front [6]. Consequently, based on fractal theory, the increase in flame velocity is directly proportional to the increase in the area of the flame front. Hence, when assessing the acceleration ability and acceleration exponent, the flame surface area emerges as a crucial parameter. The previous quantification and assessment of instability and self-acceleration in hydrogen flames have predominantly relied on 2D imaging techniques [5-10]. However, the constraints of 2D imaging techniques lie in their inability to capture the behaviour of flames in the third dimension. A 3D swinging laser sheet system has been developed in combustion studies [16–19], making the measurement of the 3D flame surface structure and area possible. The 3D swinging sheet technique enables the flame surface to be studied quantitatively in detail and provides significant insights into the self-acceleration issue.

Accurate modelling of hydrogen combustion in accident scenarios within confined spaces faces challenges due to computational costs, chemical complexity, grid resolution, and the limited availability of ad-hoc experiments to validate models [20]. Additionally, capturing the wrinkling and thickness of the flame poses a significant challenge in grid size. For Direct Numerical Simulation (DNS), thermo-diffusive instabilities in freely-propagating lean premixed hydrogen flames have been explored using high-resolution two-dimensional DNS [3]. This exploration specifically considers the effects of reactant conditions (temperature, pressure, and equivalence ratio) on resulting local flame properties (speed, thermal thickness, and reaction zone thickness). The findings indicate that the instability coefficient ω_2, which is the coefficient of the second-order term in a linear stability analysis [21], seems to be a good measure of the diffusive balance [3,4,21]. Subsequently, thermodiffusively-unstable lean premixed hydrogen flames are investigated using three-dimensional DNS with finite-rate chemical kinetics, revealing that thermo-diffusive response is stronger in 3D compared to 2D [4]. Both 2D and 3D DNS flames require validation from corresponding experimental data for a comprehensive understanding of the underlying processes.

To investigate the instability in two types of flames, we consider a planar flame characterized by a flat flame front advancing into a quiescent fresh mixture at a constant velocity. Additionally, we examine an outwardly propagating spherical flame originating from a point source and progressing into a combustible mixture within an infinite domain. This study delves into the development of 3D quasi-planar and spherical flame structures of self-accelerating premixed lean hydrogen-air mixtures using the swinging laser sheet technique. The objectives are as follows: (i) to accurately determine the reliable acceleration exponents of hydrogen-air laminar unstable flames using the 3D swinging laser sheet technique; (ii) to present instantaneous data parameters associated with the morphological characteristics (flame surface area, burned gas volume, etc.) of the flame surface, and explore the intrinsic relationship between the flame morphological characteristics due to instabilities and the acceleration exponents; (iii) to study the synergistic effects of intrinsic flame-generated turbulence and externally imposed turbulence on the flame morphological characteristics; (iv) to vary and validate the stability model parameter against experiments enables accurate prediction of flame features like wrinkling and cellular structures, ensuring robust flame stability and dynamics predictions.

2. Experimental method

2.1. MK-II combustion fan-stirred vessel

Premixed flames were ignited in a spherical combustion vessel (Fig. 1) with an internal diameter of 380 mm and three pairs of orthogonal windows, each 150 mm in diameter, for optical access. Four fans, each driven by an 8 kW electric motor, generated near-uniform isotropic turbulence in the central region of the combustion vessel. More details about the combustion vessel and its auxiliary are in [22, 23]. The turbulent root mean square (rms) velocity, u', was correlated with the fan speed N_f in rpm in [24].

2.2. 3D swinging laser sheet system

The 3D swinging laser sheet system is introduced in this section, as shown in Fig. 1. In this study, olive oil was chosen as the seeding particles with a density of 920 kg/m^3. The tracer particles are generated by a six-jet atomiser (9010F0021, Dantec), and mixed with air in the intake pipes before they are introduced into the combustion vessel. The generated olive oil droplets have a diameter $\approx$ 1 μm and a boiling temperature of about 570 K [19]. A double pulsed Nd: YAG imaging laser (DM60–532-DH, Photonics Industries) produced a 532 nm

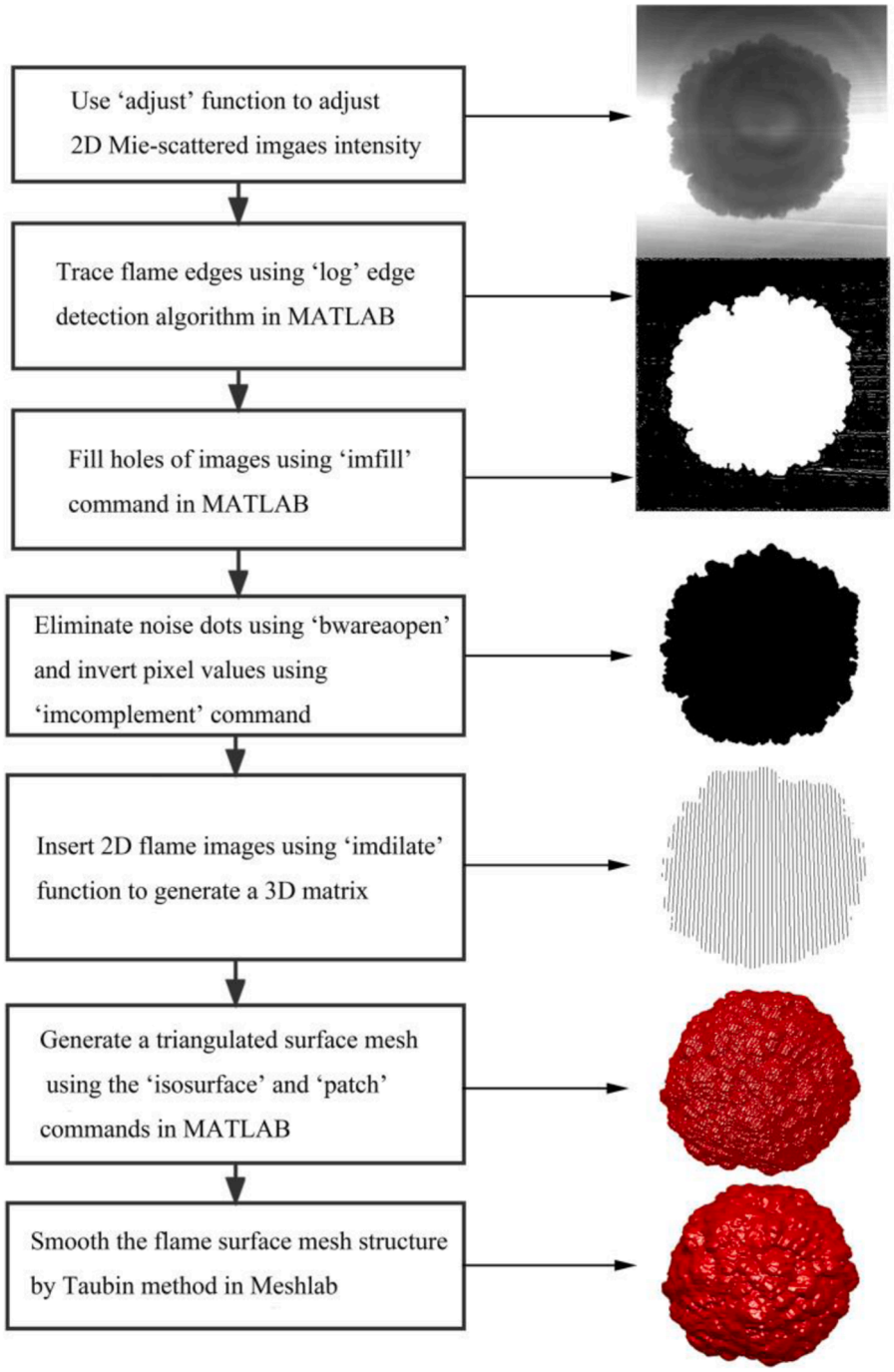

Fig. 2. Flow chart of 2D Mie-scattered flame image post-processing for 3D spherical flame reconstructions.

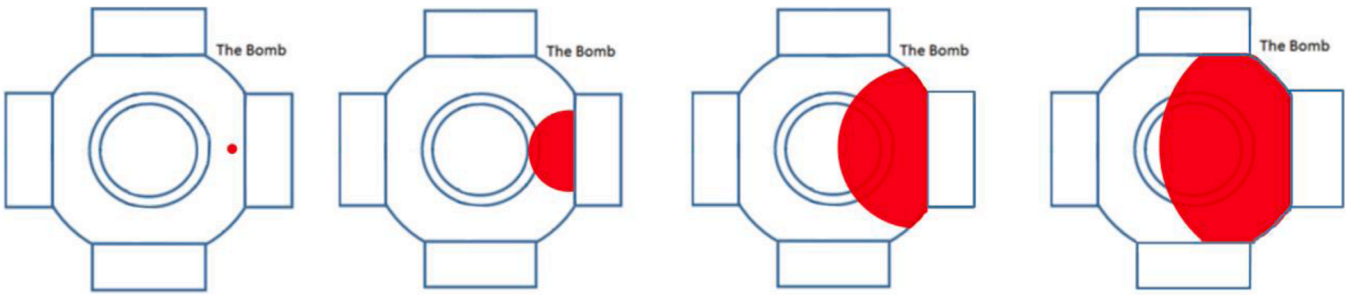

Fig. 3. The configuration and development of flame expansion.

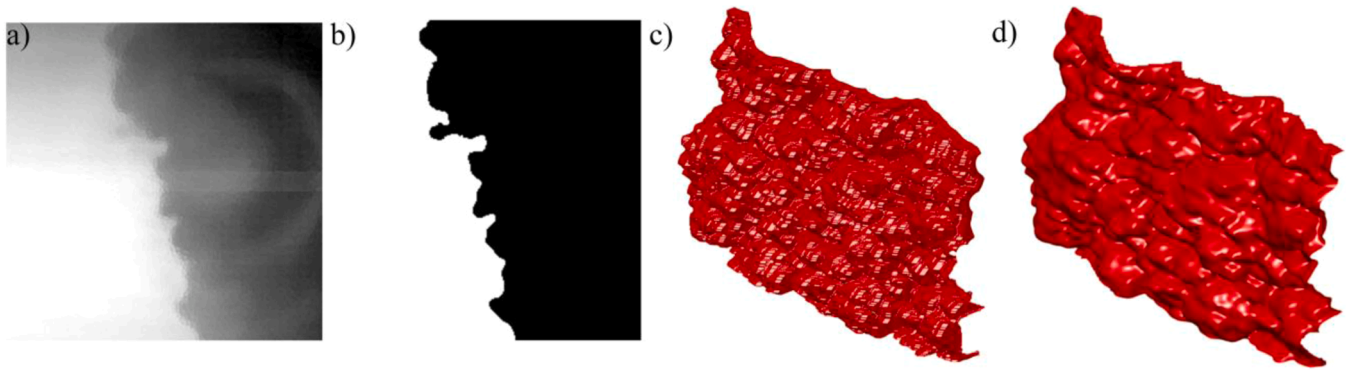

Fig. 4. Flow chart of 2D Mie-scattered flame image post-processing for 3D quasi-planar flame reconstructions. (a) flame edge detection (b) binarization (c) merging (d) smoothing.

wavelength green light laser beam with a maximum beam energy of 12mJ (pulsing at a frequency of 40 kHz). A 16-sided rotating mirror at 10 Hz was synchronized with the imaging laser using a series of optics to create multiple thin laser sheets sweeping along the vessel. A high-speed camera pointed perpendicular to the laser sheet recorded the Mie-scattering images from the tracer particles. For ignition, a New Wave solo 120 Nd:YAG laser synchronized with a 3D swinging laser sheet system was employed. Further details of laser sheet geometry and synchronization control system are available in [16–19].

2.2.1. Centrally ignited expanding spherical flames

The flow chart of the 3D reconstruction of the centrally ignited expanding spherical flame is shown in Fig. 2. The high-speed camera captured the Mie-scattered images of 512 × 512 pixels at a frequency of 40 kHz with a pixel size of 0.222 mm/pixel, depicting the burned and unburned gas mixture. Olive oil droplets would vaporize in the high-temperature burned gas and not scatter light. Consequently, the iso-surface of the flame is defined by the evaporation temperature of olive oil, approximately 570 K. Measurements of the flame surface area and its wrinkling are then conducted based on this temperature threshold.

2.2.2. Quasi-planar flame propagation

To analyze the 3D quasi-planar (nil curvature effect) flames, hydrogen-air mixtures are ignited near the wall of the experimental combustion chamber, which will result in quasi-planar flames by the time the observation window is reached, as shown in Fig. 3. This allows investigating the levels of thermos-diffusive instability in lean hydrogen flames. The high-speed camera captured a 12-bit picture pair of 256 × 256 pixels at a frequency of 40 kHz with a pixel size of 0.222 mm/pixel, enabling the examination of small sections of the wrinkled flame surface. The process of reconstructing a 3D quasi-planar flame surface is similar to that used for spherical flames, involving steps such as flame edge detection, binarization, merging, and smoothing (Fig. 4).

2.2.3. 3D reconstructed flame analysis

Surface areas were obtained by calculating the area of each triangle in the triangulated surface mesh and then summing these to yield the overall surface area of the reconstructed flame, A_{3D}. For spherical flames, the volume of each reconstruction flame, V_{3D} was obtained first by converting the triangulated surface mesh into a solid reconstruction consisting of voxels. The volume-equivalent radius is the radius of the equivalent spherical flame based on the volume of burned gas r_{3D}. The laminar equivalent mean flame area is then defined as $a_{3D} = 4\pi r_{3D}^2$. The ratio of A_{3D} to a_{3D} represents the wrinkling extent of the spherical flame. For a quasi-planar flame, a_{3D} is the cross-sectional area of the plane.

2.3. Experimental conditions

The thermal-diffusive (TD) instability of the hydrogen-air mixture is more pronounced when the mixture is leaner due to the negative Markstein number [2]. In lean hydrogen-air mixtures, the equivalence ratio of the ignition limit is approximately $\phi = 0.2$ [25]. The buoyancy effect becomes significant in mixtures with a flame speed of <0.15 m s^{-1}. Therefore, an equivalence ratio of $\phi = 0.3$ was chosen in this study for spherical flames. All experiments were conducted using a hydrogen-air mixture with an initial temperature of 360K. The temperature of the unburned gas inside the combustion chamber is assumed to be constant, as established in previous work [26].

To investigate different intensities of Darrieus-Landau (DL) instability, initial pressures of 0.1, 0.3, 0.5, 0.7, and 1.0 MPa were selected. Additionally, to study the effects of competition between the intrinsic flame-generated turbulence and external turbulence on the flame's morphological characteristics, discrete turbulence intensities (u') of 0.3 and 0.5 m s^{-1} were employed to generate relatively mild turbulence. For quasi-planar flames, an equivalence ratio of $\phi = 0.3$ was chosen at initial pressures of 0.1, 0.3, 0.5, and 1.0 MPa, while a mixture with $\phi = 0.25$ was chosen at 0.3 and 0.5 MPa.

Systematic uncertainties in the experimental setup were attributed to three primary sources: $a \pm 0.2$ % error margin in the fuel amount, $a \pm 0.05$ % error margin in pressure measurement, and $a \pm 0.7$ % error margin in temperature measurement. In the experiments, hydrogen of 99.995 % purity was employed, with the air comprising industrial oxygen and industrial nitrogen in a 21:79 molar ratio. To ensure repeatability, each experimental condition was tested three times. The standard deviation error bars were calculated as the square root of the variance, which is the sum of squared deviations divided by the number of trials. These error bars were then plotted around the mean values in all experimental results.

Despite the innovative nature of the swinging laser sheet system, various sources of error contribute to overall measurement uncertainty: (1) Laser sheet spacing and divergence: variations in laser sheet spacing and beam divergence can significantly impact the resolution and accuracy of the reconstructed 3D flame surface, affecting measurements of flame surface areas, volumes, and velocities. The use of higher-frequency lasers can enhance accuracy in the future. (2) Image processing errors: errors introduced during the binarization and edge detection processes, such as image noise and thresholding variability, can lead to significant uncertainties in the reconstructed flame structure. (3) Synchronization and control: precise synchronization between the rotating mirror and laser pulses is essential. Any misalignment can compromise the accuracy of the 3D reconstruction. (4) Seeding particles and Mie scattering: The distribution and behavior of seeding particles used for Mie scattering can vary under different initial conditions, leading to inconsistencies in flame surface measurements. (5)

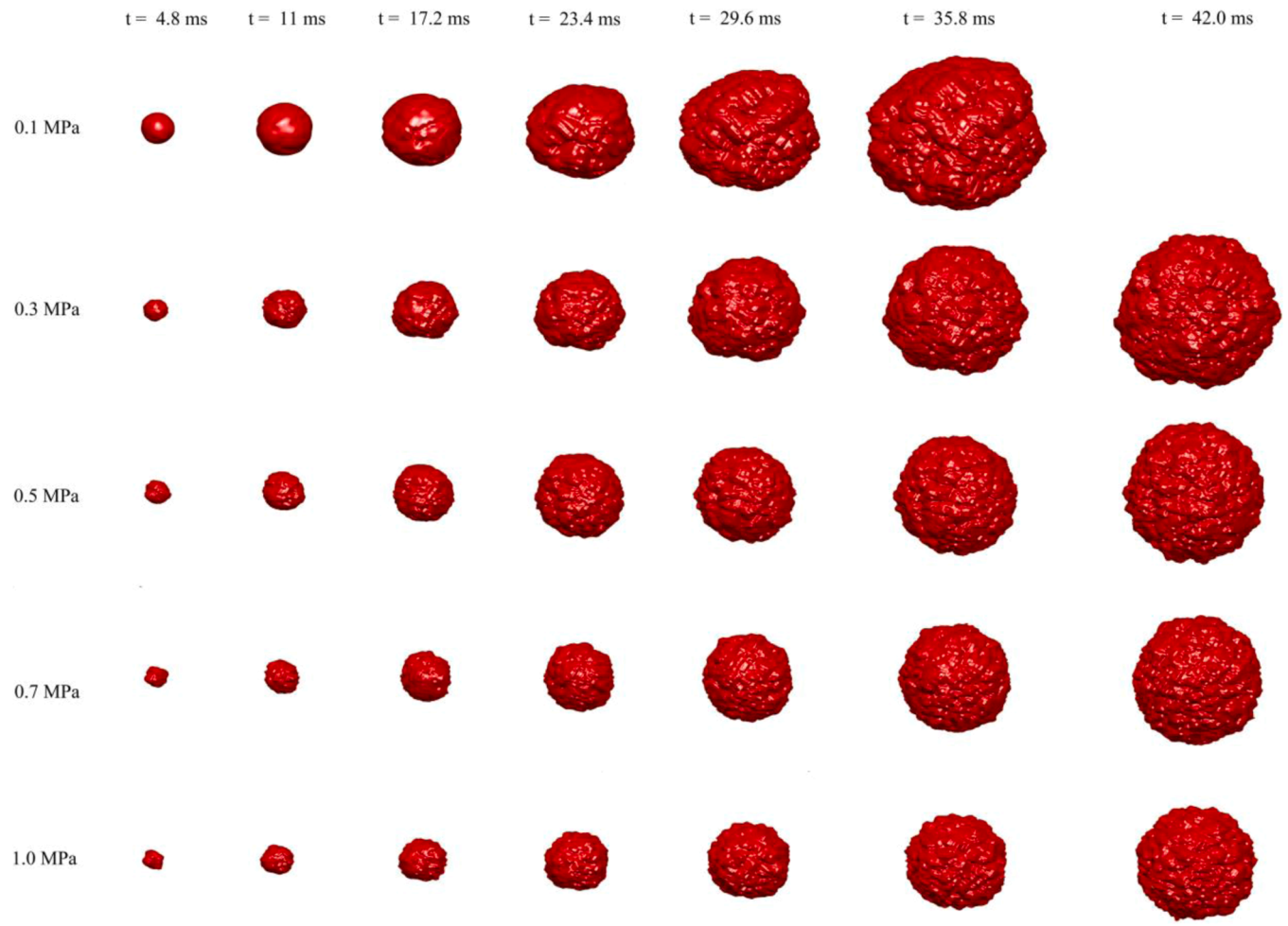

Fig. 5. Temporal developments of 3D reconstructed hydrogen-air laminar flames at, ϕ =0.3, T = 360 K and P = 0.1, 0.3, 0.5, 0.7, 1.0 MPa.

Calibration and instrumentation: calibration errors in the laser and imaging systems, as well as instrumentation errors from cameras, mirrors, and other optical components, can propagate through the measurement process and contribute to the overall uncertainty.

Instability parameters

Due to the high diffusivity of the fuel molecules, lean premixed hydrogen flame behaves thermodiffusively unstable. Specifically, when the flame surface is deformed such that it has positive curvature (centre of curvature in the products), the high mobility of the hydrogen molecules results in diffusive focusing into the hot product region, which then burns intensely, increasing the surface deformation further. Consequently, there can be significant variation of local flame speed over the surface as well as an increase in flame surface area. The thermodiffusive instability is strongly dependent on the reactant conditions (pressure, temperature and equivalence ratio), as well as the turbulent conditions.

In the linear stability analysis [21], a planar flame surface described as $F(x,t) = Ae^{\omega t + ikx}$ propagating at a speed S_n with a characteristic thickness δ (and a timescale $\tau_L = \delta/S_n$), a growth rate ω and a wavenumber k, respectively. A normalized growth rate $\widetilde{\omega}$, given by $\widetilde{\omega} = \omega\tau_L$, leads to a dispersion relation expressed as:

$$\widetilde{\omega} = \omega_{\mathrm{DL}}\widetilde{k} + \omega_2\widetilde{k}^2 \tag{2}$$

where the coefficient for the first-order term, ω_{DL}, is the Darrieus-Landau coefficient given by:

$$\omega_{\mathrm{DL}} = \frac{1}{\sigma+1}\left(\sqrt{\sigma^3+\sigma^2-\sigma}-\sigma\right) \tag{3}$$

where σ is the density ratio of the unburnt mixture to the fully burnt mixture. The coefficient for the second-order term is:

$$\omega_2 = -\left[B_1 + Ze\left(Le_{eff}-1\right)B_2 + PrB_3\right] \tag{4}$$

where B_1, B_2, B_3 account for the (de)stabilising effects of thermal, species and viscous diffusion Le_{eff}, Pr, Ze are the effective Lewis number, Prandtl number and Zel'dovich numbers. Recently, Aspden et al., [3,4] demonstrated that thermal-diffusive instability in lean premixed hydrogen can be well-characterised by a parameter ω_2 arising from classical stability analysis (e.g. [21]). Further details can be found in [3, 4,21]. The parameter ω_2 has been used well before in [3] and ultimately addresses the conditions for which the mixture Lewis number $Le < Le_0$, falls below a critical value Le_0, typically slightly less than one. Then ω_2 was replaced by an equivalent parameter ϵ in [27]

$$\epsilon = (Le_0 - Le)/(1 - Le_0) \tag{5}$$

where Le is the Lewis number of the deficient reactant, Le_0 is the critical Lewis number: $Le_0 = 1 - \frac{B_1+PrB_3}{ZeB_2}$. ϵ is a parameter that quantifies the deviation of the Lewis number from a critical value. The critical Lewis number Le_0 serves a threshold value that distinguishes between stabilizing and destabilizing thermal diffusive effects in a flame. Depending on whether the actual Lewis number (Le) is above or below Le_0, the flame can exhibit different stability characteristics: When $Le < Le_0$: The

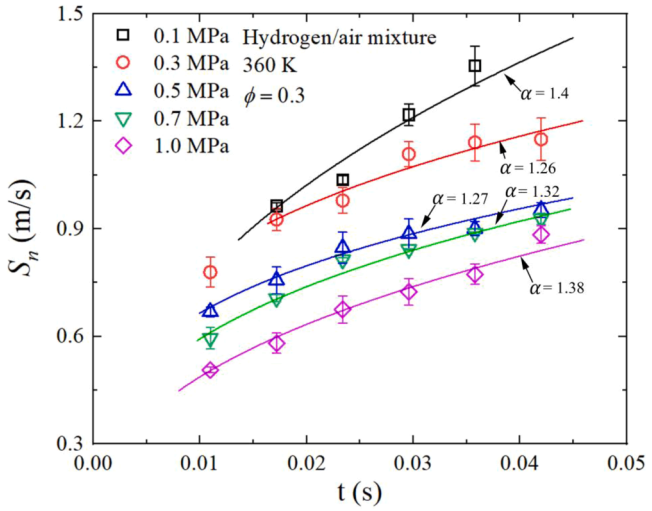

Fig. 6. Flame propagation speeds of 3D reconstructed hydrogen-air laminar flames with increasing time from ignition under different initial pressures, at ϕ = 0.3 and 360 K.

thermal diffusive effects are destabilizing, which means small-scale corrugations can grow, leading to unstable flame structures. When $Le > Le_0$: The thermal diffusive effects are stabilizing, helping to smooth out flame perturbations and stabilize the flame front.

In addition, the growth rate of hydrodynamic instability is directly proportional to the density jump across the flame and it becomes more pronounced with increasing σ [2,28]. Therefore, it is likely that σ is the most sensitive and influential parameter in triggering hydrodynamic instability. The DL coefficient, ω_{DL}, which is based on σ, serves as a robust and reliable parameter for assessing and evaluating hydrodynamic response. Furthermore, flame thickness (δ) is expected to significantly influence hydrodynamic instability for two main reasons: First, thinner flames are less affected by curvature and consequently exhibit a stronger destabilizing tendency. Second, thinner flames lead to a higher density gradient, which intensifies the development of hydrodynamic instability due to the increased strength of the induced baroclinic torque.

The calculation of flame thickness using the specified method, known as the preheat zone flame thickness, δ_k [29]:

$$\delta_k = \frac{(k/c_p)_{T^0}}{\rho_u u_{\nearrow}} \tag{6}$$

Where $(k/c_p)_{T^0}$ is the ratio of thermal conductivity and specific heat at a certain inner layer temperature, T^0. The values of T^0 for different gases are presented in [29]. This can be used for hydrogen flame since the unique feature of hydrogen flame is that the preheating zone is not completely chemically inert.

Results and discussions

The evolution of 3D laminar flame surface for hydrogen-air mixtures at $\phi = 0.3$, temperature of 360 K, and pressure ranging from 0.1 to 1.0 MPa are shown in Fig. 5. Some works have already been studied experimentally [2,6,30,31] and numerically [32,33], demonstrating that lean premixed hydrogen flames are highly susceptible to thermo-diffusive instabilities. These instabilities significantly enhance flame speed and alter flame dynamics, with critical flame radii decreasing as pressure increases. During the initial stages of flame propagation, the flame stretch rate is high and plays a stabilizing role in preventing the underlying thermo-diffusive and hydrodynamic instability, known as TD and DL instability. This initial stabilization is more prominent at higher Markstein numbers, which helps maintain a smooth flame surface [2]. However, the flame surface begins to exhibit numerous cracks after the initial smooth phase. In all cases, from 0.1 MPa to 1.0 MPa, the flame surface transitions to a completely cellular structure by $t = 23.4$ ms. As these cells grow in size, the localized stretch rate on their surfaces decreases, making the cells more prone to instabilities. A sufficiently low Markstein number, due to increased pressure, leads to more cracking and smaller cells [3].

Interestingly, at the same time, increased pressure not only makes the flame more susceptible to instability but also reduces the volume of burned gas. This suggests that elevated pressure impedes flame propagation from the start, which is in agreement with previous studies [34]. As the initial pressure increased, the mole fractions of the three active radicals (H, O, OH) declined significantly, leading to a lower laminar burning velocity. For ϕ = 0.3 (Lewis number far less than one), indicating an unstable flame, heat fluxes are subordinated in favour of mass diffusive fluxes. The imbalance in diffusive fluxes of heat and mass across the flame surfaces, along with varying local burning velocities, diminishes the spherical shape of the burned gas in the flame. Pressure variation minimally affects either *Le* or σ, but directly impacts the flame: by changing its flame thickness. Increased pressure significantly reduces the flame thickness making it more vulnerable to destabilization, which eventually leads to a highly wrinkled and irregular flame surface.

The derived flame propagation speeds using Eq. (1) are shown in Fig. 6. The experimental flame acceleration exponent, α, was evaluated by plotting the flame speed against time $S_n \sim t^{\alpha-1}$. The coefficient α is derived from the flame speed and serves as a parameter to measure the capability of flame speed acceleration. The derived acceleration exponents of flame speed in the investigations of hydrogen self-acceleration fames are consistent with previous studies using 2D imaging system [6]. However, as pressure increases from 0.3 MPa to 1.0 MPa, the acceleration exponent progressively increases from 1.26 to 1.38, with an exception at 0.1 MPa, where flame exhibits both the highest propagation speed and a greater acceleration exponent. Generally, increased pressure does lead to the earlier onset of instability, a more wrinkled flame surface area, and a higher acceleration exponent.

According to Damköhler's theory [35], in low-intensity turbulence, the premixed turbulent flame surface area A_T is augmented by the turbulent flow field, leading to a rise in the turbulent burning velocities u_t as follows:

$$u_t/u_l \sim A_T/A_L \tag{7}$$

where u_t is the stretched burning velocity, u_l is the unstretched laminar burning velocity, and A_L is the laminar flame surface area. To account for the influence of stretch on the local laminar velocity on the flame surface, Damköhler's assumption is adjusted using the parameter, I_0, as [19,36]:

$$I_0 = \frac{u_t/u_l}{A_T/A_L} \tag{8}$$

I_0 remains close to unity for premixed combustion of methane-air mixtures [19]. However, for hydrogen-air flames, the increase in burning velocity exceeds the expected rise based on the measured increase in flame surface area, with the value of I_0 up to 6. This concept is extended to an unstable spherical flame of hydrogen/air mixtures:

$$I_0 = \frac{u_n/u_l}{(A_{3D}/a_{3D})} \tag{9}$$

Here, A_{3D}/a_{3D} is the flame surface area ratio, an indication of surface area enhancement of the unstable hydrogen/air flame . The stretched laminar burning velocity including the unstable regime, u_n, is related to the stretched flame speed, S_n, by [37]:

$$u_n = \overline{\rho}_b S_n/\rho_u + r_u/(3\rho_u)(d\overline{\rho}_b/dt) \tag{10}$$

where ρ_u is the unburned gas density, ρ_b is the burned gas density, $\overline{\rho}_b$ is mean density within the radius, r_u. The second term in the right side of

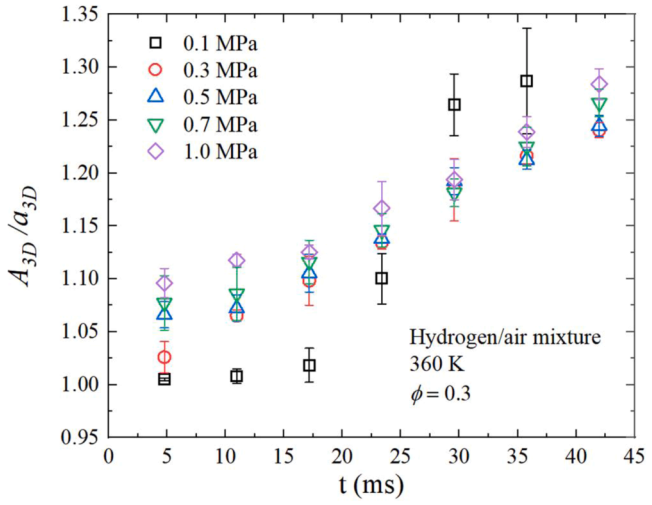

Fig. 7. Flame surface area ratio A_{3D}/a_{3D} as measured by 3D reconstruction as a function of time.

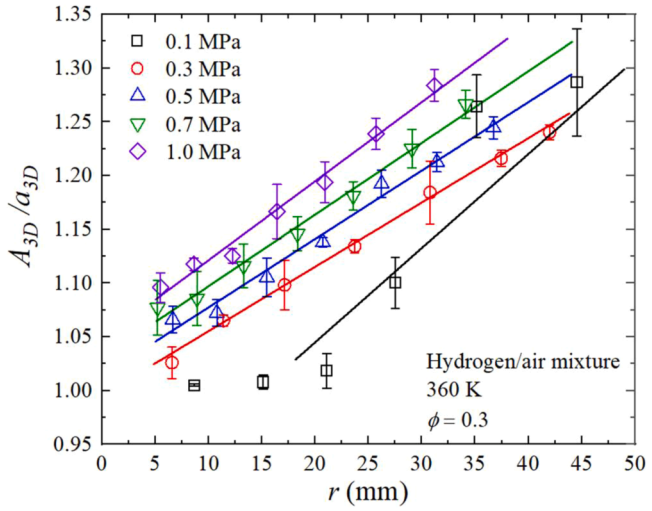

Fig. 8. Flame surface area ratio A_{3D}/a_{3D} as measured by 3D reconstruction as a function of flame radius.

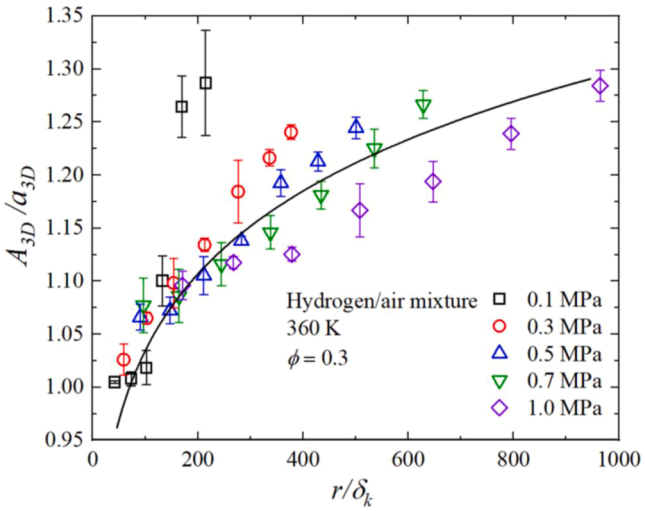

Fig. 9. The dimensionless wrinkled ratio of the flame surface under different normalized flame radii (r/δ_k). The black solid line represents the fitting curve for all data points.

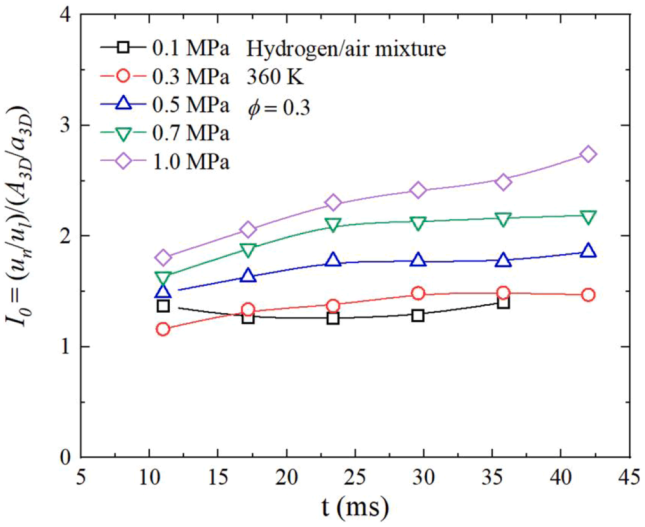

Fig. 10. Variations in I_0.

Eq. (10) declines and eventually becomes insignificant as the flame grows [19], and is neglected in this study. The values of unstretched burning velocities, u_l, are obtained from experimental data [38].

It is interesting and important to delve further into the normalized flame surface area (A_{3D}/a_{3D}) in order to gain deeper insights into the self-acceleration phenomenon. In Fig. 7, the flame surface area ratio (A_{3D}/a_{3D}) is plotted against time at $\phi = 0.3$. At 0.1 MPa, it initially remains nearly constant initially due to the smooth flame surface, then experiences a rapid increase due to intrinsic instability. For other pressures, there is a consistent tendency of (A_{3D}/a_{3D}) increasing as the flame expands over time. Additionally, at a given time, higher pressure corresponds to a higher (A_{3D}/a_{3D}). An intriguing finding is that, as mentioned earlier, the roundness of the hydrogen-air laminar flames is considerably poorer at 0.1 MPa, resulting in larger error bars compared to the elevated pressures. This reveals the chaotic nature of self-acceleration in laminar hydrogen-air mixtures under atmospheric conditions, where thermal-diffusive effects dominate.

To more accurately evaluate the extent of the wrinkling on the flame surface, it is crucial to fix the size due to the varying resolutions that different sizes produce, given the limitations of the setup. Therefore, plotting the flame surface area ratio A_{3D}/a_{3D} against the flame radius, as depicted in Fig. 8, is a more reasonable and adequate approach. It is evident that increased pressure generally results in a significantly wrinkled flame surface. The dimensionless wrinkled ratio of the flame surface and the normalized flame radius (r/δ_k) is also studied in Fig. 9 to gain a deeper understanding of the underlying mechanisms. It is observed that, despite some scatter, the black solid line generally represents the fitted curve for the entire dataset. However, two data points at atmospheric conditions (0.1 MPa) deviate from this trend. At 0.1 MPa, hydrogen flame instabilities are primarily driven by thermal-diffusive effects, which tend to form finger-like cell structures [3,4], resulting in a more irregular flame shape. This behavior indicates the chaotic nature of laminar hydrogen-air flames under atmospheric conditions, where thermal-diffusive effects dominate. As a consequence, the extent of the flame sphericity decreases at lower pressures, leading to an increase in flame surface area compared to higher pressure conditions. A potential source of this discrepancy may stem from the resolution of the Mie-scattering images and the laser repetition rate, as the current measurement precision could introduce some degree of error in the results.

Variations of I_0 is illustrated in Fig. 10, showing an approaching

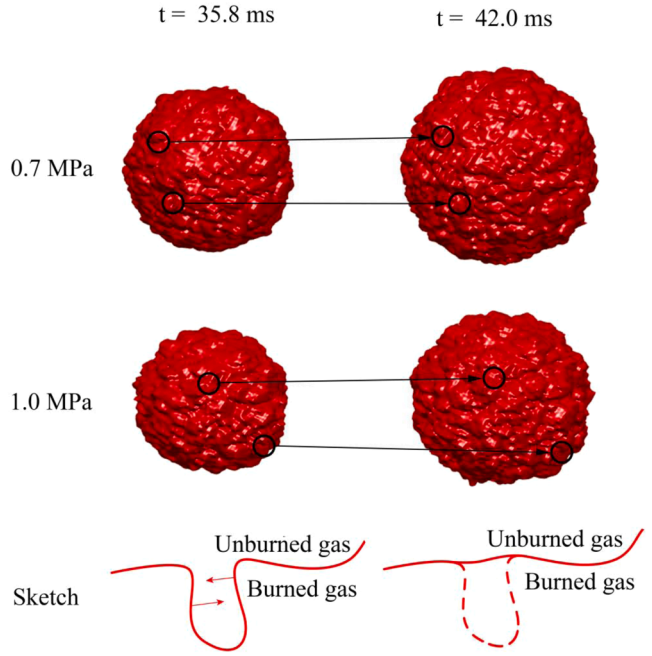

Fig. 11. Destruction of flame surface area at regions of negative curvature.

unity at 0.1 and 0.3 MPa, validating the assumption of Damköhler, which remains applicable to self-accelerating premixed hydrogen-air laminar flames. However, as pressure increases, I_0 also increases, resembling a phenomenon observed in high Karlovitz stretch factor (K) turbulent flames [19]. One possible explanation for this is that at high pressure, cells become significantly smaller, and the repetition rate of the laser may become insufficient to capture the intricate details of the flame surface. Another reason could be the distortion of surface wrinkling in regions of high negative curvature, particularly under elevated pressures, as illustrated in Fig. 11.

It is proposed that a strong outwards velocity pulse can create extra "combustion turbulence" as a result of the combined effects of a fast-burning rate and rapid volumetric expansion [15]. To acquire deeper insights into the turbulence arising from flame instability and its impact on flame morphological characteristics, we introduced a controlled amount of external turbulence for comparative analysis. Fig. 12 illustrates the temporal evolution of the 3D flame surface of hydrogen-air mixtures under varying root mean square (rms) velocities (0, 0.3, 0.5 m s^{-1}) at $\phi = 0.3$, $P = 0.1$ MPa, and $T = 360$ K. Even with very mild turbulence ($u' = 0.3$ m s^{-1}), it becomes apparent that externally-imposed turbulence can substantially wrinkle the flame surface, surpassing the effect of intrinsic flame cellularity. This effect becomes even more pronounced at $u' = 0.5$ m s^{-1}. Correspondingly, the values of A_{3D}/a_{3D} presented in Fig. 13 reveal the expected trend of increasing A_{3D}/a_{3D} with higher u'. In comparison, A_{3D}/a_{3D} under the influence of mild external turbulence ($u' = 0.3$ and 0.5 m s^{-1}) far exceeds the levels achieved by

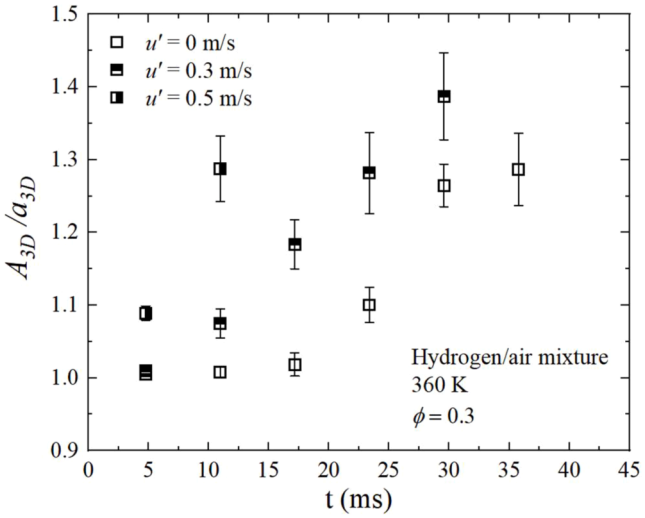

Fig. 13. Flame surface area ratio A_{3D}/a_{3D} as measured by 3D reconstruction as a function of time for different rms velocities at $\phi = 0.3$, $T = 360$ K and $P = 0.1$ MPa.

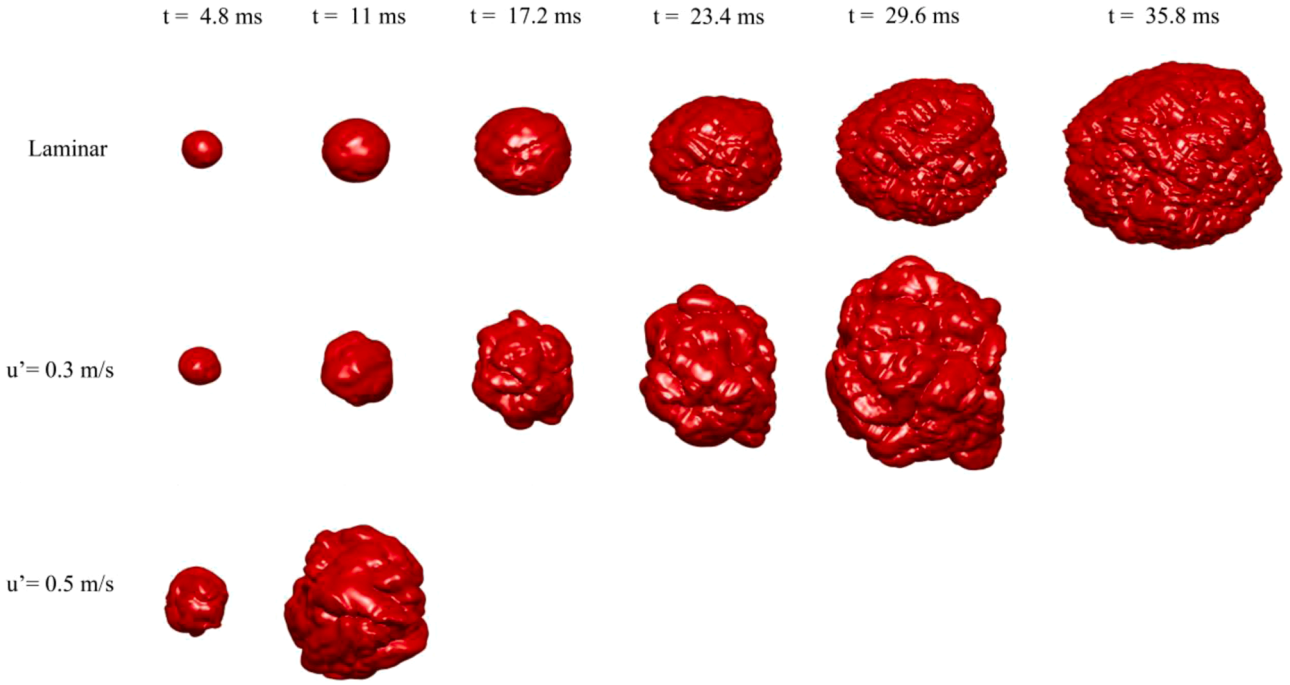

Fig. 12. Temporal developments of 3D reconstructed laminar hydrogen-air flames at $\phi = 0.3$, $T = 360$ K and $P = 0.1$ MPa under different rms velocities.

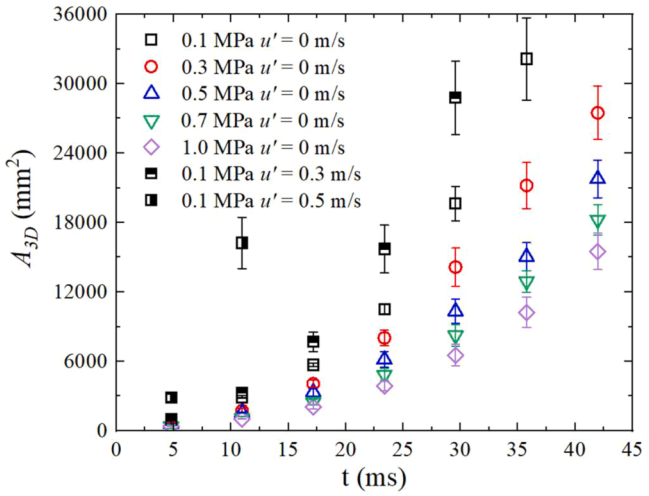

Fig. 14. Flame surface area of hydrogen-air flames with increasing time from ignition at $\phi = 0.3$, $T = 360$ K.

intrinsic instability.

The wrinkling of the flame surface may result from both intrinsic cellularity due to DL instability arising from elevated pressures or gas strain induced by external turbulence. However, they yield significantly different outcomes in the context of premixed hydrogen-air unstable outwardly propagating spherical flames, affecting parameters such as burned gas volume, flame surface area radius, and speed. As depicted in Fig. 14, increased pressure tends to hinder flame propagation, while external turbulence has the opposite effect, accelerating flame propagation. This reinforces that the distinct mechanisms responsible for surface folding due to DL or TD instability, or the influence of external turbulence, are distinct. Intrinsic cellularity due to DL or TD instability stems from the nonequilibrium of diffusive fluxes of heat and mass, or the susceptibility of flame to destabilization due to reduced thickness. In contrast, chaotic external turbulence generates gas strain with different sizes and directions, resulting in the wrinkling of the flame surface. It is widely accepted that turbulence increases the flame surface area, subsequently raising the burning rate. This can also be attributed to the synergistic effects between thermos-diffusive instabilities and turbulence, resulting in higher fuel consumption rates per flame surface area, with the instabilities forming finger-like structures that enhanced flame displacement speed in curved flame segments [39].

The three-dimensional flame surface of the quasi-planar laminar flame of hydrogen-air mixtures at $\phi = 0.3$, as depicted in Fig. 15, clearly illustrates that higher pressure leads to a more wrinkled flame surface with smaller cells. Previous modelling studies [3,4], have indicated that mean local flame speeds increase in correlation with the thermal-diffusive response parameter ω_2. This parameter proves to be an excellent indicator of thermal-diffusive strength and its capacity to predict the degree of thermos-diffusive response in freely-propagating and turbulent flame. The relationship between the flame surface area ratio of the freely-propagating quasi-planar flame at the center of the combustion vessel (with a flame radius of approximately 160 mm) and the instability parameter ω_2 is illustrated in Fig. 16. It is evident that higher values of ω_2 correspond to higher values of $\boldsymbol{A}_{3D}/\boldsymbol{a}_{3D}$, indicating that stronger thermal-diffusive (TD) instability plays a pivotal role in altering the morphology of the flame surface, making it more wrinkled.

Furthermore, the values of A_{3D}/a_{3D} and ϵ are also plotted in this study in Fig. 17, revealing a discernible linear relationship between them. This is rather intuitive as ϵ measures the distance of the mixture Lewis number from the critical Lewis number (Le_0). The greater this distance the more the thermo-diffusive effects are destabilizing. The underlying reason is that the wavelength of the flame surface tends to decrease with ϵ (i.e. as the Le decreases), allowing for a greater number of unstable perturbation wavelengths to be accommodated within the flame domain. As a result, the flame wrinkling increases.

Conclusions

Simultaneous 3D measurements capturing the evolution and morphological characteristics of hydrogen-air laminar unstable flames were conducted in a constant volume vessel using the advanced 3D swinging laser sheet technique. The application of the 3D swing laser sheet technique allows for a re-examination of flame speed self-acceleration, offering the capability to study the three-dimensional morphological characteristics of flame and directly quantify the flame

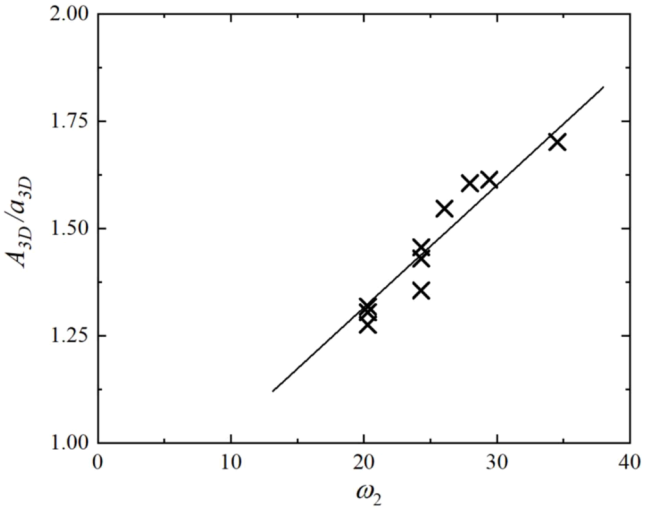

Fig. 16. The wrinkled flame surface area ratio of freely-propagating quasi-planar flame at the flame radius of 160 mm as functions of instability parameter ω_2.

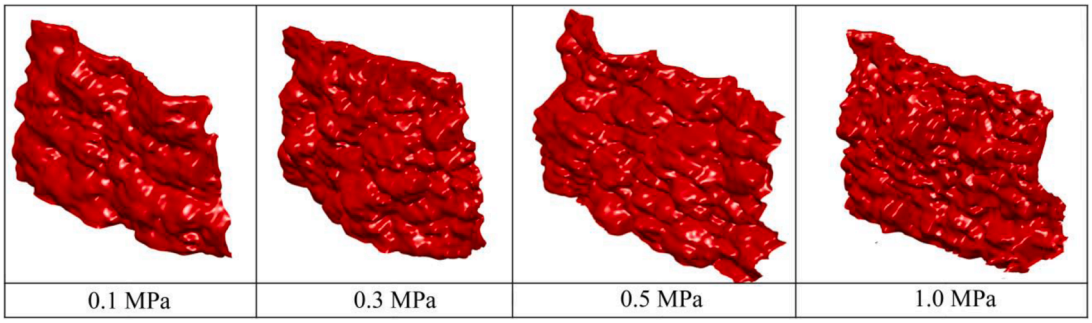

Fig. 15. Flame morphological characteristics of 3D reconstructed quasi-planar laminar flame surface of hydrogen-air mixtures under various initial pressures, at $\phi = 0.3$ and 360 K.

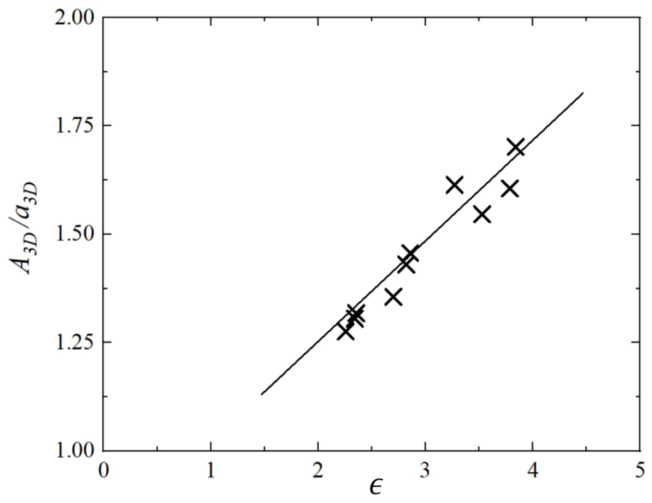

Fig. 17. The wrinkled flame surface area ratio of freely-propagating quasi-planar flame at the flame radius of 160 mm as functions of instability parameter ϵ.

surface area. Through this technique, diverse insights into the acceleration phenomenon can be gained.

Exploring the effects of instability on flame speed self-acceleration, pressure dependencies were investigated. As the pressure rises from 0.3 MPa to 1.0 MPa, hydrodynamic (DL) instability intensifies due to reduced flame thickness. This leads to a gradual escalation in the acceleration exponent, increasing from 1.26 to 1.38. The cellularity caused by DL or TD instability is a consequence of high pressure alone. The extent of the flame surface wrinkling is proportional to the increasing flame burning velocity at low pressures but becomes invalid for high pressures. The annihilation of surface wrinkles may occur, especially under high pressures in regions of strong negative curvature or at locations where the flame surface is indented. The effects of external turbulence, even at relatively low levels, on the wrinkling extent of the flame surface are much stronger than those of intrinsic instability. While gas strain from external turbulence and intrinsic cellularity caused by Darrieus-Landau (DL) instability due to increased pressure can induce flame surface wrinkling, the elevated pressure impedes flame propagation, whereas external turbulence accelerates it. This can be attributed to the synergistic effects between thermo-diffusive instabilities and turbulence, resulting in higher fuel consumption rates per flame surface area, with the instabilities forming finger-like structures that enhance flame displacement speed in curved flame segments. In the case of a quasi-planar flame, the ratio of the wrinkled flame surface area increases as pressure rises. The linear model parameters ϵ and ω_2 prove to be excellent indicators of the strength of thermal-diffusive instability in planar flames, demonstrating a linear correlation with the ratio of the wrinkled flame surface area.

Novelty and significance

This research enhances our comprehension of the development and morphological traits of premixed hydrogen-air unstable flames by employing three-dimensional measurements. A distinguishing feature of this study is the novel methodology employed for three-dimensional reconstructions of flames, facilitating the determination of flame-burned gas volume and the area of wrinkled flame surfaces. Elevated pressure levels are anticipated to lead to higher acceleration exponents and increased wrinkling of flame surfaces in centrally ignited expanding spherical flames, as well as quasi-planar flames. The parameters ϵ and ω_2 serve as effective descriptors of intrinsic instabilities in hydrogen flames.

Author contributions

Yu Xie: Formal analysis, Methodology, Visualization, Original draft. Junfeng Yang: Review and editing, Project administration, Funding acquisition, Supervision. Pervez Ahmed: Experimental support, Review and editing. Benjamin John Alexander Thorne: Experimental support. Xiaojun Gu: Review and editing.

Declaration of competing interest

The authors declare that they have no known competing financial interests or personal relationships that could have appeared to influence the work reported in this paper.

Acknowledgements

The authors thank to EPSRC (grant no. EP/W002299/1) for the financial support. Yu Xie acknowledges the China Scholarship Council and the University of Leeds for a joint PhD scholarship (CSC202008350141).

References

[1] A.L. Pillai, S. Inoue, T. Shoji, S. Tachibana, T. Yokomori, R. Kurose, Investigation of combustion noise generated by an open lean-premixed H2/air low-swirl flame using the hybrid LES/APE-RF framework, Combust. Flame 245 (2022) 112360.
[2] Y. Xie, M.E. Morsy, J. Li, J. Yang, Intrinsic cellular instabilities of hydrogen laminar outwardly propagating spherical flames, Fuel 327 (2022) 125149.
[3] T.L. Howarth, A.J. Aspden, An empirical characteristic scaling model for freely-propagating lean premixed hydrogen flames, Combust. Flame 237 (2022) 111805.
[4] T.L. Howarth, E.F. Hunt, A.J. Aspden, Thermodiffusively-unstable lean premixed hydrogen flames: phenomenology, empirical modelling, and thermal leading points, Combust. Flame 253 (2023) 112811.
[5] C.R. Bauwens, J.M. Bergthorson, S.B. Dorofeev, Experimental study of spherical-flame acceleration mechanisms in large-scale propane–air flames, Proc. Combust. Inst. 35 (2) (2015) 2059–2066.
[6] Y. Xie, M.E. Morsy, J. Yang, Self-acceleration and global pulsation of unstable laminar hydrogen-air flames, Fuel 353 (2023) 129182.
[7] Y.A. Gostintsev, A.G. Istratov, Yu.V. Shulenin, Self-similar propagation of a free turbulent flame in mixed gas mixtures, Combust. Explos. Shock Waves (1989) 563–569.
[8] F. Wu, G. Jomaas, C.K. Law, An experimental investigation on self-acceleration of cellular spherical flames, Proc. Combust. Inst. 34 (2013) 937–945.
[9] S. Yang, A. Saha, F. Wu, C.K. Law, Morphology and self-acceleration of expanding laminar flames with flame-front cellular instabilities, Combust. Flame 171 (2016) 112–118.
[10] J. Huo, A. Saha, Z. Ren, C.K. Law, Self-acceleration and global pulsation in hydrodynamically unstable expanding laminar flames, Combust. Flame 194 (2018) 419–425.
[11] A.N. Lipatnikov, V.A. Sabelnikov, S. Nishiki, T. Hasegawa, Does flame-generated vorticity increase turbulent burning velocity? Phys. Fluids 30 (8) (2018).
[12] S. Chaudhuri, A. Saha, C.K. Law, On flame–turbulence interaction in constant-pressure expanding flames, Proc. Combust. Inst. 35 (2015) 1331–1339.
[13] B.D. Videto, D.A. Santavicca, Flame-turbulence interactions in a freely-propagating, premixed flame, Combust. Sci. Technol. 70 (1–3) (1990) 47–73.
[14] S. Chaudhuri, A. Saha, C.K. Law, On flame–turbulence interaction in constant-pressure expanding flames, Proc. Combust. Inst. 35 (2) (2015) 1331–1339.
[15] D. Bradley, M. Lawes, M.E. Morsy, Combustion-induced turbulent flow fields in premixed flames, Fuel 290 (2021) 119972.
[16] M.R. Harker, T. Hattrell, M. Lawes, C.G.W. Sheppard, N. Tripathi, R. Woolley, Measurements of the three-dimensional structure of flames at low turbulence, Combust. Sci. Technol. 184 (2012) 1818–1837.
[17] B.J.A. Thorne, Development of a 3D Laser Imaging System and Its Application in Studies of Turbulent Flame Structure (Doctoral Dissertation, University of Leeds, 2017.
[18] S.P. Ahmed, Studies of Turbulent Burning Rates and Flame Structures Using 3D Optical Measurement Techniques (Doctoral Dissertation, University of Leeds, 2019.
[19] P. Ahmed, B. Thorne, M. Lawes, S. Hochgreb, G.V. Nivarti, R.S. Cant, Three dimensional measurements of surface areas and burning velocities of turbulent spherical flames, Combust. Flame 233 (2021) 111586.
[20] F. Nicolás-Pérez, F.J.S. Velasco, R.A. Otón-Martínez, J.R. García-Cascales, A. Bentaib, N. Chaumeix, Capabilities and limitations of Large Eddy Simulation with perfectly stirred reactor assumption for engineering applications of unsteady, hydrogen combustion sequences, Eng. Applic. Comput. Fluid Mech. 15 (1) (2021) 1452–1472.
[21] M. Matalon, C. Cui, J.K. Bechtold, Hydrodynamic theory of premixed flames: effects of stoichiometry, variable transport coefficients and arbitrary reaction orders, J. Fluid Mech. 487 (2003) 179.

[22] Y. Xie, J. Li, J. Yang, R. Cracknell, Laminar burning velocity blending laws using particle imaging velocimetry, Appl. Energy Combust. Sci. 13 (2023) 100114.
[23] Y. Xie, A. Lu, J. Li, J. Yang, C. Zhang, M.E. Morsy, Laminar burning characteristics of coal-based naphtha, Combust. Flame 249 (2023) 112625.
[24] D. Bradley, M. Lawes, M.E. Morsy, Measurement of turbulence characteristics in a large scale fan-stirred spherical vessel, J. Turbul. 20 (3) (2019) 195–213.
[25] D. Bradley, Fundamentals of Lean Combustion, Lean Combustion Academic Press, 2008, pp. 19–53.
[26] R.D. Mumby, Experimental Characterisation of Fuel Blends (Doctoral Dissertation, University of Leeds, 2016.
[27] F. Creta, P.E. Lapenna, R. Lamioni, N. Fogla, M. Matalon, Propagation of premixed flames in the presence of Darrieus–Landau and thermal diffusive instabilities, J. Fluid Mech. 216 (2020) 256–270.
[28] O.C. Kwon, G. Rozenchan, C.K. Law, Cellular instabilities and self-acceleration of outwardly propagating spherical flames, Proc. Combust. Inst. 29 (2) (2002) 1775–1783.
[29] J. Göttgens, F. Mauss, N. Peters, Analytic approximations of burning velocities and flame thicknesses of lean hydrogen, methane, ethylene, ethane, acetylene, and propane flames, Sympos. (Int.) Combust. 24 (1992) 129–135.
[30] J. Beeckmann, R. Hesse, S. Kruse, A. Berens, N. Peters, H. Pitsch, M. Matalon, Propagation speed and stability of spherically expanding hydrogen/air flames: experimental study and asymptotics, Proc. Combust. Inst. 36 (1) (2017) 1531–1538.
[31] Y. Xie, J. Yang, X. Gu, Flame wrinkling and self-disturbance in cellularly unstable hydrogen-air laminar flames, Combust. Flame 265 (2024) 113505.
[32] L. Berger, A. Attili, H. Pitsch, Intrinsic instabilities in premixed hydrogen flames: parametric variation of pressure, equivalence ratio, and temperature. part 1-dispersion relations in the linear regime, Combust. Flame 240 (2022) 111935.
[33] L. Berger, A. Attili, H. Pitsch, Intrinsic instabilities in premixed hydrogen flames: parametric variation of pressure, equivalence ratio, and temperature. Part 2–Non-linear regime and flame speed enhancement, Combust. Flame 240 (2022) 111936.
[34] A.K. Marwaan, J. Yang, A.S. Tomlin, H.M. Thompson, G. de Boer, K. Liu, M. E. Morsy, Laminar burning velocities and Markstein numbers for pure hydrogen and methane/hydrogen/air mixtures at elevated pressures, Fuel 354 (2023) 129331.
[35] G. Damköhler, Der einfluss der turbulenz auf die flammengeschwindigkeit in gasgemischen, Zeitschrift für Elektrochemie und angewandte physikalische Chemie 46 (11) (1940) 601–626.
[36] A. Bagdanavicius, P.J. Bowen, D. Bradley, M. Lawes, M.S. Mansour, Stretch rate effects and flame surface densities in premixed turbulent combustion up to 1.25 MPa, Combust. Flame 162 (2015) 4158–4166.
[37] D. Bradley, P.H. Gaskell, X.J. Gu, Burning velocities, Markstein lengths, and flame quenching for spherical methane-air flames: a computational study, Combust. Flame 104 (1–2) (1996) 176–198.
[38] D. Bradley, M. Lawes, K. Liu, S. Verhelst, R. Woolley, Laminar burning velocities of lean hydrogen–air mixtures at pressures up to 1.0 MPa, Combust. Flame 149 (2007) 162–172.
[39] L. Berger, A. Attili, H. Pitsch, Synergistic interactions of thermodiffusive instabilities and turbulence in lean hydrogen flames, Combust. Flame 244 (2022) 112254.

Further reading

[40] Z. Liu, V.R. Unni, S. Chaudhuri, R. Sui, C.K. Law, A. Saha, Self-turbulization in cellularly unstable laminar flames, J. Fluid Mech. 917 (2021).